JOURNAL OF COMPUTATIONAL PHYSICS **132,** 91–107 (1997)
ARTICLE NO. CP965625

Correction of Conservative Euler Solvers for Gas Mixtures

P. Jenny, B. Müller,*,[1] and H. Thomann

Institut für Fluiddynamik, Swiss Federal Institute of Technology (ETH), CH-8092, Zürich, Switzerland
E-mail: *b.mueller@math.utwente.nl

Received May 24, 1996; revised November 25, 1996

Conservative Euler solvers for gas mixtures produce numerical errors near contact discontinuities, if the temperature and the ratio of specific heats are not constant there. For mixtures of perfect gases, a simple correction of the total energy per unit volume is proposed to avoid these errors. This is done in a physical way and only the total energy looses some of its conservativity. Numerical simulations of contact discontinuity convection, a shock tube problem, and shock-interface interactions in 1D and 2D yield much more accurate solutions, if the correction is applied. The straightforward extension to 3D is outlined.

1. INTRODUCTION

For the computation of reactive flow in combustion and in hypersonic aerothermodynamics, the conservation laws of species mass, momentum, and energy have to be solved [10, 12]. Accurate and robust upwind discretizations of the inviscid fluxes have been generalized from perfect gas to thermochemical nonequilibrium flows [1, 9, 18]. If such conservative schemes are employed, numerical inaccuracies and oscillations can occur at contact discontinuities even if diffusion and chemical reactions are not considered [1, 5]. The numerical problem was explained in [1, 7]: If a contact discontinuity separating two fluids enters a control volume, the conservative formulation leads to numerical mixing of the fluid due to the averaging process. If the two fluids have different γ and temperature, the averaged pressure will be different from the originally constant pressure.

Colella, Glaz, and Ferguson [3] derived a multifluid Eulerian algorithm from a corresponding Lagrangian method. Their volume-of-fluid method assures pressure equilibrium among the fluid components, thereby avoiding the numerical problem of conventional conservative schemes at contact discontinuities just mentioned.

Karni [7] solved the problem by employing a non-conservative formulation, which accounts for the conservation errors up to the truncation error. That second-order non-conservative scheme was employed by Quirk and Karni [13] to simulate the interactions of plane shock waves with cylindrical gas bubbles contained in air using adaptive mesh refinement. In another approach, Karni [8] solved the conservation laws augmented by the non-conservative energy equation, identified the vicinity of the contact discontinuity, and switched there from a conservative formulation to a non-conservative one with regard to the energy equation. Toro [17] used a non-conservative scheme, except for the vicinity of shock waves where the discretization is switched to a conservative scheme. However, since most flow solvers employ conservative formulations [1, 9, 18] to guarantee, e.g., correct shock speeds and to take advantage of the geometric flexibility of the finite volume concept, a simple correction procedure of conservative schemes will probably be more useful than changing the whole formulation.

Abgrall [2] solves the conservative equations with the classical multispecies Roe scheme, but adds an additional transport equation for $1/(\gamma - 1)$ to update γ. Considering that the sum of the mass fractions must be one he gets together with the equation for γ in mixtures of two perfect gases two linear equations for two unknowns. However, it is not clear how to treat a problem with three or more species where the number of unknowns is higher than the number of equations. In combustion with complex chemistry a small change of the mass fraction of a radical can lead to inaccurate results.

We have used physical reasoning to find a simple solution to the problem for mixtures of perfect gases: We determine the volume flow over each cell interface by decoding the conservative variables from the fluxes. In each cell, we adjust the in- and outgoing volumes such that we arrive at a constant pressure in all fluids. That process turns out to be equivalent to volume averaging the pressure. Thereby the convection of the internal energy is taken into account. Adding the kinetic energy flux and the rate of work done by the pressure forces, we arrive at a simple correction of the total energy per unit volume.

Algorithmically, the correction can be easily imple-

[1] Current address: Faculty of Applied Mathematics, University of Twente, NL-7500 AE Enschede, The Netherlands.

0021-9991/97 $25.00

mented in the explicit finite volume discretization of the energy equation: the internal energy density at the old time level

$$(\rho e)^n = \frac{p^n}{\gamma^n - 1}$$

is replaced by

$$\frac{p^n}{\gamma^{n+1} - 1}$$

and the internal energy flux difference

$$\Delta(\rho u e)^n = \Delta\left(\frac{up}{\gamma - 1}\right)^n$$

is replaced by

$$\frac{\Delta(up)^n}{\gamma^{n+1} - 1}.$$

The flow variables at the cell interfaces have to be decoded from the numerical flux, if they are not directly given by the numerical flux evaluation. γ^{n+1}, the ratio of specific heats in the considered cell at the new time level, is determined by the species continuity equations. For a perfect gas with constant γ, the correction vanishes as it should be, because then no problems at the contact discontinuities arise.

This correction step can easily be added to explicit conservative multi-component flow solvers after each time step. It is extendable to 2D and 3D. The conservativity error is shown to be zero, if the temperature or γ is constant. No negative effects of some loss of conservativity in the energy equation have been encountered, if the temperature and γ are not constant.

In Section 2, the Euler equations for a mixture of perfect gases are stated. The conservative Euler solver is described in Section 3. In Section 4, the origin of the error at contact discontinuities is outlined. Sections 5 and 6 describe the correction algorithm of a conservative Euler solver in 1D and its extension to multi-dimension, respectively. The results presented in Section 7 show that applying the correction leads to more accurate results. Conclusions are given in Section 8.

2. EULER EQUATIONS FOR A GAS MIXTURE

We restrict our presentation for simplicity to only two species and one dimension in space, but there is no difference to problems with several species in two or three dimensions, as we shall see in Section 6. The conservation laws of species mass, momentum, and energy for inviscid 1D flow of a mixture of two perfect gases constitute the 1D Euler equations for two species. Expressed in differential form they read

$$\frac{\partial \mathbf{U}}{\partial t} + \frac{\partial \mathbf{f}}{\partial x} = 0, \tag{1}$$

where

$$\mathbf{U} = \begin{pmatrix} \rho_1 \\ \rho_2 \\ \rho u \\ \rho E \end{pmatrix} \quad \text{and} \quad \mathbf{f} = \begin{pmatrix} \rho_1 u \\ \rho_2 u \\ \rho u^2 + p \\ u(\rho E + p) \end{pmatrix}. \tag{2}$$

The vector of the conservative variables $\mathbf{U}$ contains ρ_1 and ρ_2, i.e., the mass densities of species 1 and 2, respectively, density $\rho = \rho_1 + \rho_2$, velocity u, and the total energy per unit mass $E = e + u^2/2$, where e is the internal energy per unit mass. The pressure p appearing in the flux vector $\mathbf{f}$ is given by the equations of state for a perfect gas mixture

$$p = (\gamma - 1)\left(\rho E - \frac{\rho}{2} u^2\right) = \rho R_s T, \tag{3}$$

where γ, R_s, and T denote the ratio of specific heats, specific gas constant, and temperature, respectively. R_s, the specific heat at constant pressure c_p, and $\gamma = c_p/c_v$ are given by

$$R_s = \frac{R_u}{\rho} \sum_{j=1}^{2} \frac{\rho_j}{W_j} \qquad c_p = \frac{1}{\rho} \sum_{j=1}^{2} \rho_j c_{p_j} \qquad \gamma = \frac{c_p}{c_p - R_s}. \tag{4}$$

R_u denotes the universal gas constant. W_1 and W_2, the molecular weights of species 1 and 2, are in general not equal. c_{p_1} and c_{p_2}, the specific heats at constant pressure of the species, are assumed to be constant.

3. CONSERVATIVE EULER SOLVER

An explicit conservative discretization leads to

$$\mathbf{U}_i^{n+1} = \mathbf{U}_i^n - \frac{\Delta t}{\Delta x}(\mathbf{f}_{i+1/2}^n - \mathbf{f}_{i-1/2}^n) \tag{5}$$

which is typical for finite volume methods. $\mathbf{U}_i^n$ is an approximation of the cell average $(1/\Delta x) \int_{x_{i-1/2}}^{x_{i+1/2}} \mathbf{U}(x, n\,\Delta t)\, dx$ in cell i at the time $n\,\Delta t$. The numerical fluxes $\mathbf{f}_{i+1/2}$ and $\mathbf{f}_{i-1/2}$ at the right and left cell interfaces $x_{i\pm1/2}$, respectively, approximate the fluxes $(1/\Delta t) \int_{n\,\Delta t}^{(n+1)\,\Delta t} \mathbf{f}(x_{i\pm1/2}, t)\, dt$. Here the numerical fluxes are determined with Roe's approximate Riemann solver for multiple species [14, 9]:

$$\mathbf{f}_{i+1/2} = \frac{1}{2}[\mathbf{f}(\mathbf{U}_{i+1/2,R}) + \mathbf{f}(\mathbf{U}_{i+1/2,L}) - |\hat{\mathbf{A}}_{i+1/2}|(\mathbf{U}_{i+1/2,R} - \mathbf{U}_{i+1/2,L})].$$

$\hat{\mathbf{A}}_{i+1/2}$ is the Jacobian matrix of $\mathbf{f}$ evaluated at the Roe average of $\mathbf{U}_{i+1/2,L}$ and $\mathbf{U}_{i+1/2,R}$. For first order, $\mathbf{U}_{i+1/2,L} = \mathbf{U}_i$ and $\mathbf{U}_{i+1/2,R} = \mathbf{U}_{i+1}$.

To achieve second order in space, the MUSCL ansatz with the minmod limiter has been employed. It is important that the primitive variables are used for the extrapolation to avoid problems with wrong pressures when employing the conservative variables. Thus the Riemann problem at the right cell interface $x_{i+1/2}$ is determined by the following values of $\mathbf{V} = (\rho, \rho_1/\rho, u, p)$,

$$\mathbf{V}_{i+1/2,L} = \mathbf{V}_i + \text{minmod}\left(\frac{\mathbf{V}_i - \mathbf{V}_{i-1}}{x_i - x_{i-1}}, \frac{\mathbf{V}_{i+1} - \mathbf{V}_i}{x_{i+1} - x_i}\right)(x_{i+1/2} - x_i)$$

$$V_{i+1/2,R} = \mathbf{V}_{i+1} - \text{minmod}\left(\frac{\mathbf{V}_{i+2} - \mathbf{V}_{i+1}}{x_{i+2} - x_{i+1}}, \frac{\mathbf{V}_{i+1} - \mathbf{V}_i}{x_{i+1} - x_i}\right)(x_{i+1} - x_{i+1/2})$$

with

$$\text{minmod}(a, b) = \begin{cases} a & \text{if } (|a| \le |b|) \text{ and } (ab > 0) \\ b & \text{if } (|b| < |a|) \text{ and } (ab > 0) \\ 0 & \text{if } (ab \le 0) \end{cases}$$

and x_i the location of the cell midpoint.

4. ORIGIN OF THE ERROR AT CONTACT DISCONTINUITIES

We consider a contact discontinuity with species 1 and 2 on the left and right sides, respectively, propagating from left to right at constant velocity u and constant pressure p. At time $t = n\,\Delta t$, let the contact discontinuity coincide with a certain cell interface $x_{i-1/2}$. Thus, the Riemann problem is defined by the left and right states (Fig. 1a). Suppose we choose $\sigma = u\,\Delta t/\Delta x < 1$ for stability reasons, the contact discontinuity will move from $x_{i-1/2}$ to the location $x_{i-1/2} + u\,\Delta t$ in cell i during one time step (Fig. 1b). Thus, the exact fluxes during the next time step are here $\mathbf{f}_{i+1/2} = \mathbf{f}(\mathbf{U}_r) = u\mathbf{U}_r + p(0, 0, 1, u)^T$ and $\mathbf{f}_{i-1/2} = \mathbf{f}(\mathbf{U}_l) = u\mathbf{U}_l + p(0, 0, 1, u)^T$. We obtain from (5) with Godunov's or Roe's first order methods, which coincide at contact discontinuities and shocks,

$$\mathbf{U}_i^{n+1} = \mathbf{U}_r - \sigma(\mathbf{U}_r - \mathbf{U}_l) = \Big(\sigma\rho_l, (1-\sigma)\rho_r, u\rho_i^{n+1}, \sigma(\rho e)_l + (1-\sigma)(\rho e)_r + \frac{u^2}{2}\rho_i^{n+1}\Big)^T \quad (6)$$

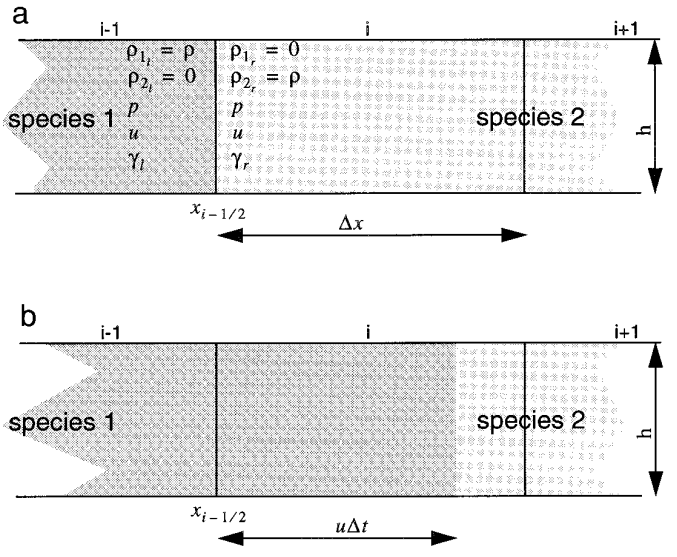

FIG. 1. (a) Riemann problem of a contact discontinuity at the left interface. (b) Contact discontinuity at $t = \Delta t$ ($p_l = p_r$).

with $\rho_i^{n+1} = \rho_{1_i}^{n+1} + \rho_{2_i}^{n+1} = \sigma\rho_l + (1-\sigma)\rho_r$.

The partial densities $\rho_{1_i}^{n+1}$ and $\rho_{2_i}^{n+1}$ show that for $0 < \sigma < 1$ the contact discontinuity is smeared, because it is captured and not tracked. However, we are more concerned about velocity and pressure. Clearly, $u_i^{n+1} = u$, but

$$p_i^{n+1} = (\gamma_i^{n+1} - 1)\left(\rho_i^{n+1}E_i^{n+1} - \frac{u^2}{2}\rho_i^{n+1}\right) = p(1 + \varepsilon_p), \quad (7)$$

where

$$\varepsilon_p = \frac{p_i^{n+1}}{p} - 1 = \frac{\sigma\rho_l R_1 + (1-\sigma)\rho_r R_2}{\sigma\rho_l c_{v1} + (1-\sigma)\rho_r c_{v2}}\left(\frac{\sigma}{\gamma_1 - 1} + \frac{1-\sigma}{\gamma_2 - 1}\right) - 1$$
$$= \frac{\sigma(1-\sigma)(\rho_l R_1 - \rho_r R_2)}{\sigma\rho_l c_{v1} + (1-\sigma)\rho_r c_{v2}}\left(\frac{1}{\gamma_2 - 1} - \frac{1}{\gamma_1 - 1}\right).$$

Using the equations of state for a perfect gas, $\rho R_s = p/T$ and $p/(\rho c_v) = T(\gamma - 1)$, we obtain for the relative pressure error

$$\varepsilon_p = \sigma(1-\sigma)\frac{(T_r - T_l)(\gamma_1 - \gamma_2)}{\sigma(\gamma_2 - 1)T_r + (1-\sigma)(\gamma_1 - 1)T_l}. \quad (8)$$

Thus, the error in pressure after one time step of the conservative Euler solver (5) is zero, if at least one of the following conditions holds:

- the contact discontinuity does not move, i.e., $\sigma = 0$,
- the contact discontinuity moves to the next cell interface, i.e., $\sigma = 1$,

• the temperatures on both sides are equal, i.e., $T_l = T_r$.

• the ratios of specific heats of the species are equal, i.e., $\gamma_1 = \gamma_2$.

Similar investigations were made in [1, 7]. Here the role of the temperature in ε_p is realized. If $0 < \sigma < 1$, $T_l \neq T_r$, and $\gamma_1 \neq \gamma_2$, the conservative Euler solver does not maintain constant pressure, but yields the relative pressure error ε_p.

Relating p_i^{n+1} to twice the dynamic pressure ρu^2 shows that the pressure error becomes more significant for low Mach numbers M since $(p_i^{n+1} - p)/(\rho u^2) = \varepsilon_p/(\gamma M^2)$. In the second time step, the pressure error ∂p induces velocity errors $\partial u \sim \pm \partial p/(\rho c)$ propagating up- and downstream, respectively, due to the acoustic disturbance. Thereby, also the velocity becomes contaminated. Our first numerical example in Section 7 will illustrate these errors.

5. THE CORRECTION ALGORITHM

To apply the present correction algorithm, the flow variables at the cell interfaces have to be known. Therefore, Subsection 5.1 explains how to decode the conservative variables, if only the flux is known, e.g., Roe's flux. However, if the flow variables are provided by the numerical flux evaluation, e.g., Godunov's method, the reader can directly proceed to Subsection 5.2. There, the total energy per unit volume ρE is corrected to maintain constant pressure and therefore also constant velocity over a contact discontinuity, if the ratios of specific heats and the temperatures on both sides differ. Thereby, a conservation error is introduced, which is analyzed in Subsection 5.3.

5.1. *Flow over the Cell Interfaces*

Suppose the integral over the cell interface at $x_{i+1/2}$ (Fig. 1b) $\int_0^h \mathbf{f}(x_{i+1/2}, y, t)\, dy$ is approximated by $\mathbf{F} = \mathbf{f}_{i+1/2}h$ with the numerical flux $\mathbf{f}_{i+1/2}$, which depends on the conservative variables in the neighboring cells $\mathbf{U}_i$, $\mathbf{U}_{i+1}$, etc. Knowing $\mathbf{F} = (F_1, F_2, F_3, F_4)^T = \mathbf{f}_{i+1/2}h$ and the functional dependence of the flux $\mathbf{f}$ on the conservative variables $\mathbf{U}$ from Eq. (2), we look for the root of the equation $\mathbf{F} = \mathbf{f}(\mathbf{U})h$ which provides us with the conservative variables at the considered cell interface.

The numerical flux $\mathbf{f}_{i+1/2}$ needs not to be Roe's but it can be any consistent one. Note that with Roe's flux, except for $\mathbf{U}_L = \mathbf{U}_R$, the Roe average $\hat{\mathbf{U}}$ does not yield the conservative variables $\mathbf{U}$ at the interface but the state for which

$$\mathbf{f}(\mathbf{U}_r) - \mathbf{f}(\mathbf{U}_l) = \mathbf{A}(\hat{\mathbf{U}})(\mathbf{U}_r - \mathbf{U}_l)$$

nor does $\mathbf{A}^{-1}(\hat{\mathbf{U}})\mathbf{f}_{i+1/2} = \mathbf{A}^{-1}(\hat{\mathbf{U}})\mathbf{A}(\mathbf{U})\mathbf{U}$ yield $\mathbf{U}$.

$\mathbf{F} = \mathbf{f}(\mathbf{U})h$ corresponds to four equations for the four unknowns ρ_1, ρ_2, ρu, and ρE:

$$F_1 = \rho_1 u h \tag{9}$$

$$F_2 = \rho_2 u h \tag{10}$$

$$F_3 = \rho u^2 h + p h \tag{11}$$

$$F_4 = u(\rho E + p)h. \tag{12}$$

If u is not zero, we get with Eqs. (4), (9), and (10),

$$(\gamma - 1)^{-1} = \frac{c_p}{R_s} - 1 = \frac{F_1 c_{p_1} + F_2 c_{p_2}}{R_u(F_1/W_1 + F_2/W_2)} - 1. \tag{13}$$

If u is zero, there is no need in evaluating γ or one of the other variables, as the flux in the energy equation is zero (e.g., Eqs. (22) and (31) below).

With Eqs. (9) and (10) we get

$$\rho u = \frac{F_1 + F_2}{h}. \tag{14}$$

The pressure is obtained using Eqs. (11) and (14),

$$p = \frac{F_3}{h} - \frac{(F_1 + F_2)^2}{\rho h^2}. \tag{15}$$

Equation (3) yields

$$\rho E = \frac{p}{\gamma - 1} + \frac{\rho}{2} u^2. \tag{16}$$

Inserting ρE given by (16) in Eq. (12) and replacing the pressure and velocity by (15) and (14), respectively, we get a quadratic equation for ρ:

$$\begin{aligned} 0 = {} & \frac{F_4}{F_1 + F_2}\rho^2 + \frac{-\gamma F_3}{(\gamma - 1)h}\rho \\ & + \frac{(F_1 + F_2)^2}{h^2}\frac{\gamma + 1}{2(\gamma - 1)} = a\rho^2 + b\rho + c. \end{aligned} \tag{17}$$

If the discriminant

$$D = 4F_4\left(\frac{\gamma + 1}{2(\gamma - 1)}\right)\frac{F_1 + F_2}{h^2} - \left(\frac{\gamma F_3}{(\gamma - 1)h}\right)^2 = 4ac - b^2 \tag{18}$$

is negative, we have two solutions, of the form

$$\rho^{\pm} = \frac{-b \pm \sqrt{b^2 - 4ac}}{2a}.$$

To figure out whether the larger or the smaller root is the physical one, we first check the larger one $\rho = \rho^+$,

$$\rho > \frac{-b}{2a} = \frac{\gamma u(\rho^2 u^2 + \rho p)}{2u(\gamma - 1)(\rho E + p)}$$

which turns out to be equivalent to $M^2 < 1$, where M is the Mach number. The smaller root $\rho = \rho^-$ corresponds to $M^2 > 1$. Thus, $\rho = \rho^+$, if we have subsonic flow, and $\rho = \rho^-$, if we have supersonic flow. If the discriminant D is zero, there is no ambiguity in the solution of Eq. (17). $D = 0$ corresponds to sonic flow $M = 1$. But if the discriminant is positive, there exist complex roots of Eq. (17). Then

$$-D = b^2 - 4ac = \frac{1}{(\gamma - 1)^2}(\gamma\rho u^2 + \gamma p)^2$$

$$- 2\frac{\gamma + 1}{\gamma - 1}(\rho^2 u^2 E + \rho u^2 p) < 0$$

leads to

$$\left(\frac{1}{M^2} - 1\right)^2 < 0.$$

As $(1/M^2 - 1)^2$ cannot be negative, the solution of Eq. (17) is nonphysical, if D is positive. Such a nonphysical result would not occur, if we applied an exact Riemann solver, e.g., Godunov's, or an approximate one like Pandolfi's, see [11] (except for a compression wave approximated by a converging fan with a sonic point at the interface), which yield the flow state at the cell interface to calculate the flux. However, with Roe's approximate Riemann solver, such a nonphysical result can occur in expansion fans, since the approximation of a fan by a discontinuity can lead to errors. Sod's shock tube problem ($p_l/p_r = 10$, $\rho_l/\rho_r = 8$, $u_l = u_r = 0$, $\gamma = 1.4$) provides an example, where Roe's approximate Riemann solver yields $D > 0$ at the diaphragm. Other problems with Roe's approximate Riemann solver in expansion fans are the necessity of an entropy fix to avoid expansion shocks [6] and the failure of linearizations near low densities [4]. If D is larger than zero, the correction procedure outlined in subsection 5.2 is not used. But since the problem of conservative Euler solvers for gas mixtures can only occur at contact discontinuities, no correction is necessary in expansion fans provided there is no interaction with a contact discontinuity.

Summarizing, the solution of Eq. (17) reads

$$\rho = \begin{cases} \text{complex} & \text{if } (D > 0) \\ \dfrac{-b + \sqrt{b^2 - 4ac}}{2a} & \text{if } (D \le 0) \text{ and } (M \le 1) \\ \dfrac{-b - \sqrt{b^2 - 4ac}}{2a} & \text{if } (D \le 0) \text{ and } (M > 1). \end{cases} \quad (19)$$

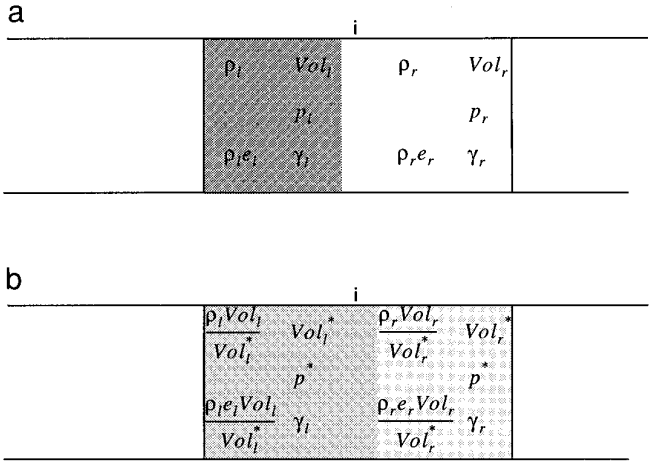

FIG. 2. (a) General situation at $t = \Delta t$ ($p_l \neq p_r$). (b) Modification of volumes at $t = \Delta t$ to achieve $p_l = p_r$.

Since in general $D < 0$, we usually have two solutions, one subsonic and one supersonic. We need an additional criterion to choose the relevant one. For simplicity, we decided to determine the Mach number approximately from the Roe average $M \approx \hat{M} = \hat{u}/\hat{c}$. According to our experience, the approximation of M by $\hat{M}$ has worked well for all test cases. The situation encountered here is similar to isentropic outflow from a stagnation chamber: for a given mass flow we usually have two solutions, one subsonic and one supersonic. If the mass flow is equal to the critical mass flow, we have one solution at sonic condition. If the mass flow is larger than the critical mass flow, we have no solution, to be precise, no steady 1D solution [16].

Having determined γ with Eq. (13), ρ with Eq. (19), and ρu with Eq. (14), we can figure out p and ρE with Eqs. (15) and (16), respectively. Knowing u, ρ_1, and ρ_2 can be determined with Eqs. (9) and (10), respectively, if $u \neq 0$. Thus, we can describe the fluid flowing through each side of the control volume.

5.2. *Correction of Total Energy per Unit Volume*

Figures 1 and 2 illustrate the basic idea of the correction algorithm. The rectangular box represents the cell. We consider a flow in a tube of height h with constant pressure and velocity. Let's assume that there is a contact discontinuity at the left side of cell i which separates two fluids with different ratios of specific heats and with different temperatures (Fig. 1a). After one time step one part of cell i is filled with the fluid on the left of the contact discontinuity and one part with the fluid on the right of the contact discontinuity (Fig. 1b). If we average the conservative variables and figure out the pressure with the laws of perfect gas mixtures, we get a pressure different from p according to Eq. (7) (excluding a situation, where the relative pressure error in Eq. (8) is zero).

However, if we modify the calculation of the internal energy assuming the ratios of specific heats to be equal to the cell averaged value γ_i^{n+1}, i.e., by replacing $(\rho e)_{l,r} = p/(\gamma_{l,r} - 1)$ by $p/(\gamma_i^{n+1} - 1)$, we obtain $p_i^{n+1} = (\gamma_i^{n+1} - 1)(\rho e)_i^{n+1} = (\gamma_i^{n+1} - 1)[\sigma p/(\gamma_i^{n+1} - 1) + (1 - \sigma)p/(\gamma_i^{n+1} - 1)] = p$.

To generalize the problem, we look at a situation where we have two regions with different pressures in a cell (Fig. 2a). The volumes occupied by the fluids on the left and the right sides are $Vol_l = hu\,\Delta t$ and $Vol_r = h(\Delta x - u\,\Delta t)$. Instead of figuring out the average pressure with the averaged conservative variables and the perfect gas law, we adapt the volumes Vol_l and Vol_r in order to have the same pressure p in the modified volumes Vol_l^* and Vol_r^*. The velocity u is assumed to be constant in the whole cell (Fig. 2b).

We imagine the contact discontinuity to be a piston that is free to adjust to a position so that the pressure is equal on both sides. Requiring in addition that the internal energies in Vol_l^* and Vol_r^* are the same as in Vol_l and Vol_r, respectively, we get the following conditions for Vol_l^* and Vol_r^*:

$$(\gamma_l - 1)\frac{Vol_l}{Vol_l^*}(\rho e)_l = \frac{Vol_l}{Vol_l^*}p_l = p^*$$

$$(\gamma_r - 1)\frac{Vol_r}{Vol_r^*}(\rho e)_r = \frac{Vol_r}{Vol_r^*}p_r = p^*.$$

Using $Vol_r^* = Vol - Vol_l^*$, we obtain from these equations

$$Vol_l^* = \frac{p_l Vol_l Vol}{p_l Vol_l + p_r Vol_r} \tag{20}$$

and therefore we get

$$p^* = \frac{p_l Vol_l + p_r Vol_r}{Vol}. \tag{21}$$

Equation (21) is easily extendable to more than two volumes. We assume that the amount of $\rho e Vol$ which was in Vol at the beginning of the time step keeps constant if Vol changes to $Vol_a = Vol - Vol_l - Vol_r$, where Vol_l and Vol_r are the volumes of the fluid which flows in during the time step at the left and right sides of the cell, respectively. Then we obtain for Vol_a the pressure $p_a = pVol/Vol_a$ where p denotes the pressure in the cell at the beginning of the time step. Substituting this in

$$p^* = \frac{p_l Vol_l + p_a Vol_a + p_r Vol_r}{Vol}$$

we obtain

$$p^* = \frac{p_l Vol_l + pVol + p_r Vol_r}{Vol}.$$

If we have a flow out of the volume at either side of the cell, the corresponding volume Vol_l or Vol_r in the equation above becomes negative. Expressing Vol_l and Vol_r by $u_l h\,\Delta t$ and $-u_r h\,\Delta t$, respectively, we obtain

$$p_i^* = p_i^n - \frac{\Delta t}{\Delta x}\Delta(up) \tag{22}$$

with

$$\Delta(.) = (.)_r^n - (.)_l^n = (.)_{i+1/2}^n - (.)_{i-(1/2)}^n.$$

The velocity and the pressure have to be figured out for each side to evaluate the pressure p^*. It turns out that the present procedure to determine the pressure p^* near a contact discontinuity leads to the same result as many multifluid Lagrangian–Eulerian procedures after the Lagrangian step (according to [3]). But the advantage of our algorithm is that there is no need to track the contact discontinuity. Further we need no additional differential equations and only the discretization of the energy equation has to be slightly modified.

Equation (22) can also be viewed as originating in the explicit discretization of

$$\frac{\partial p}{\partial t} + \frac{\partial (up)}{\partial x} \tag{23}$$

by

$$\frac{p_i^{n+1} - p_i^n}{\Delta t} + \frac{\Delta(up)}{\Delta x} \tag{24}$$

if we set Eq. (24) equal to

$$\frac{p_i^{n+1} - p_i^*}{\Delta t} \tag{25}$$

to define the ''convected'' pressure p_i^*. Now we use the product rule to express the conservative form of the convection of the internal energy $\rho e = p/(\gamma - 1)$ in nonconservative form

$$\frac{\partial}{\partial t}\left(\frac{p}{\gamma - 1}\right) + \frac{\partial}{\partial x}\left(\frac{up}{\gamma - 1}\right) = \frac{1}{\gamma - 1}\left[\frac{\partial p}{\partial t} + \frac{\partial (up)}{\partial x}\right] + p\left[\frac{\partial}{\partial t}\left(\frac{1}{\gamma - 1}\right) + u\frac{\partial}{\partial x}\left(\frac{1}{\gamma - 1}\right)\right]. \tag{26}$$

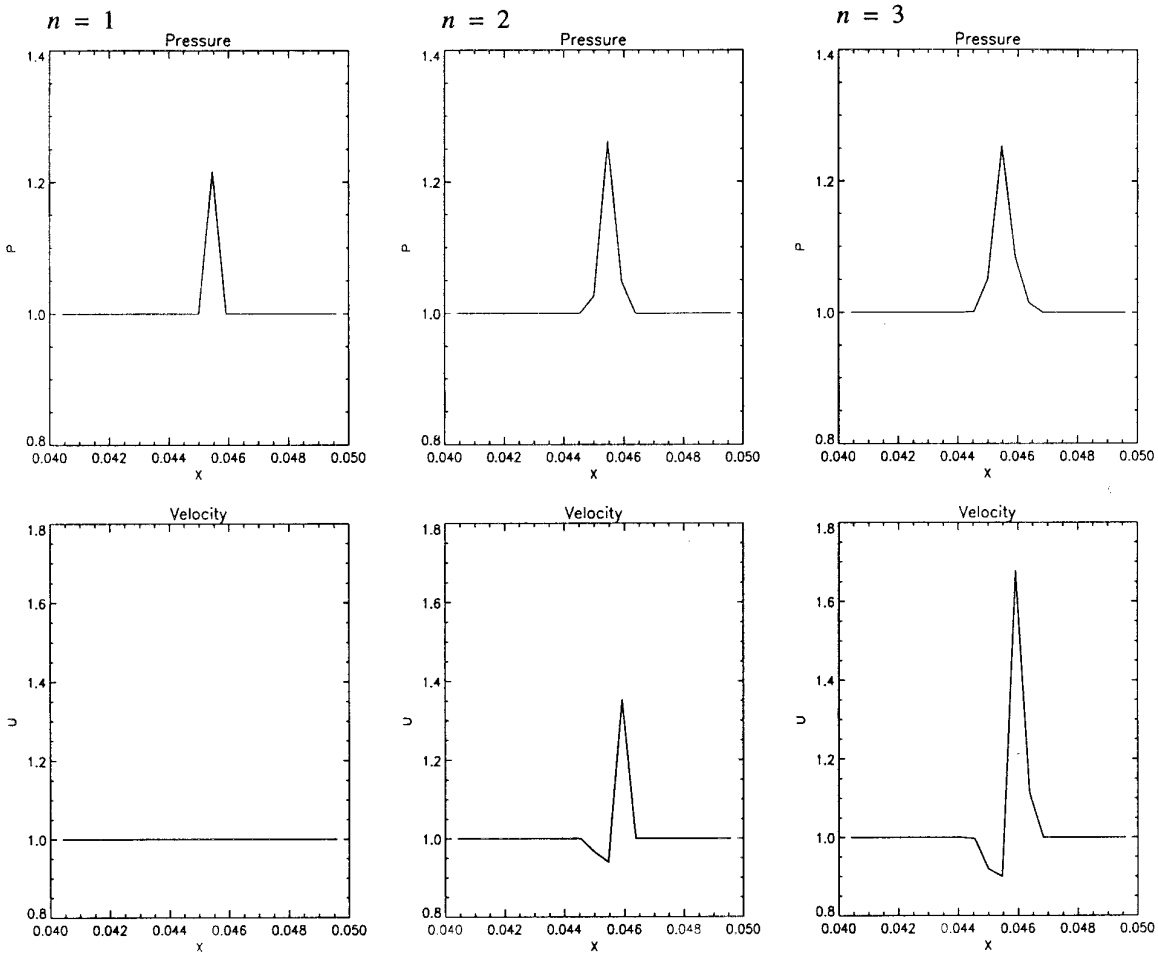

FIG. 3. Convection problem with two species without correction.

The right hand side of Eq. (26) simplifies, because the second term in brackets vanishes:

$$\frac{\partial}{\partial t}\left(\frac{1}{\gamma-1}\right)+u\frac{\partial}{\partial x}\left(\frac{1}{\gamma-1}\right)=0. \tag{27}$$

Equation (27) holds, as γ is convected with the flow. Abgrall [2] uses (27) to update γ. Then, we discretize the convection of the internal energy

$$\frac{\partial \rho e}{\partial t}+\frac{\partial(\rho u e)}{\partial x} \tag{28}$$

in the energy equation not by discretizing the conservative form (i.e., the left hand side of (26)), but because of (27) by discretizing the first term of the non-conservative form (i.e., the first term on the right hand side of (26)) using (24) and equivalently (25),

$$\frac{1}{\gamma_i^{n+1}-1}\left(\frac{p_i^{n+1}-p_i^n}{\Delta t}+\frac{\Delta(up)}{\Delta x}\right)=\frac{1}{\gamma_i^{n+1}-1}\frac{p_i^{n+1}-p_i^*}{\Delta t}. \tag{29}$$

Employing here γ_i^{n+1}, i.e., the cell averaged ratio of specific heats at the new time level, with a conservative scheme guarantees constant pressure at a contact discontinuity. Using $\rho E=\rho e+\rho u^2/2$, the energy equation reads

$$\frac{\partial \rho e}{\partial t}+\frac{\partial \frac{\rho u^2}{2}}{\partial t}+\frac{\partial \rho u e}{\partial x}+\frac{\partial \frac{\rho u^3}{2}}{\partial x}+\frac{\partial up}{\partial x}=0. \tag{30}$$

Until now we have only considered the convection of the internal energy, i.e., the first and the third terms of Eq. (30), but not the convection of the kinetic energy (second and fourth terms) and the rate of work done by the pressure forces (fifth term).

With (29) and conventional explicit discretizations for

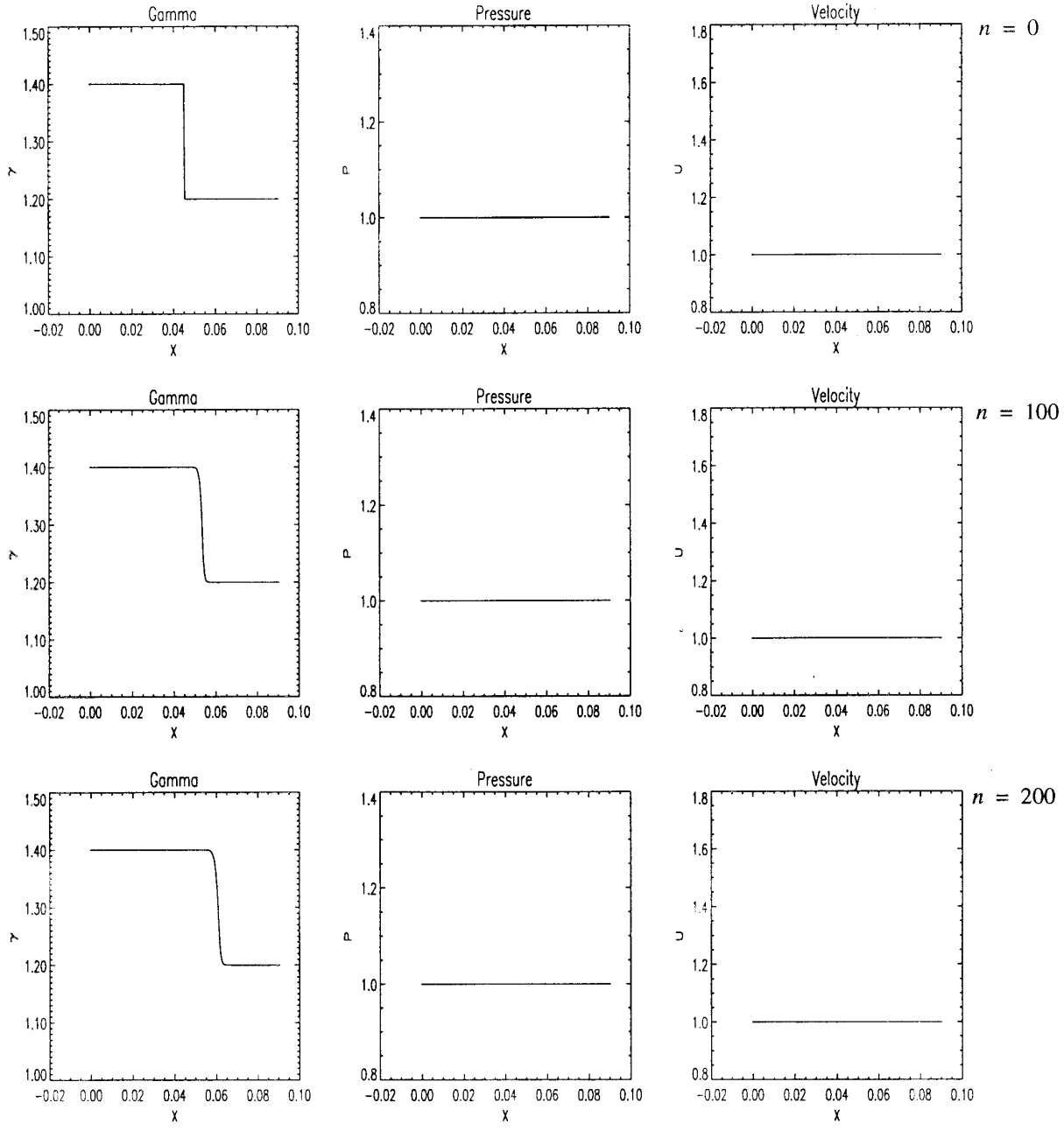

FIG. 4. Convection problem with two species with correction.

the other terms, we obtain for the corrected total energy per unit volume for inviscid flow of perfect gas mixtures

$$(\rho E)_i^c = \frac{p_i^{n+1}}{\gamma_i^{n+1}-1} + \frac{1}{2}(\rho u^2)_i^{n+1} = \frac{p_i^*}{\gamma_i^{n+1}-1} + \frac{1}{2}(\rho u^2)_i^n - \frac{\Delta t}{\Delta x}\Delta\left(\frac{1}{2}\rho u^3 + up\right). \tag{31}$$

To compute $(\rho E)_i^c$ we have to know ρ, u, and p at the cell interfaces. Here, the decoding of the flow variables from the numerical fluxes comes into play (cf. Subsection 5.1.).

For the Navier Stokes equations we have also to consider the heat flux q and the work done by the viscous forces

$$\Delta(\rho E)_i^v = \frac{\Delta t}{\Delta x}\Delta(\tau\cdot u - q)$$

and for the nonequilibrium chemistry the heat release

$$\Delta(\rho E)_i^s = \Delta t\, \dot{q}_i,$$

where τ is the stress tensor and $\dot{q}$ is the heat release rate due to the chemical reactions. Thus we calculate the corrected energy from:

$$(\rho E)_{i_{corr}}^{n+1} = (\rho E)_i^c + \Delta(\rho E)_i^v + \Delta(\rho E)_i^s. \tag{32}$$

5.3. *Error Analysis*

$(\rho E)_{i_{cons}}^{n+1}$ and $(\rho E)_{i_{corr}}^{n+1}$ are the total energies per unit volume at the time level $n+1$ derived with a conservative formulation and the corrected one, respectively. For the time integration the explicit Euler scheme has been employed.

$$(\rho E)_{i_{corr}}^{n+1} = \frac{p_i^*}{\gamma_i^{n+1}-1} - \frac{\Delta t}{\Delta x}\Delta(up) + \left(\frac{\rho}{2}u^2\right)_i^n - \frac{\Delta t}{\Delta x}\Delta\left(\frac{\rho}{2}u^3\right)$$

$$(\rho E)_{i_{cons}}^{n+1} = (\rho e)_i^n - \frac{\Delta t}{\Delta x}\Delta(u\rho e) - \frac{\Delta t}{\Delta x}\Delta(up) + \left(\frac{\rho}{2}u^2\right)_i^n - \frac{\Delta t}{\Delta x}\Delta\left(\frac{\rho}{2}u^3\right).$$

Now we can derive the difference between these two total energies per unit volume:

$$\begin{aligned}(\rho E)_{i_{error}}^{n+1} &= (\rho E)_{i_{corr}}^{n+1} - (\rho E)_{i_{cons}}^{n+1} = \frac{p_i^*}{\gamma_i^{n+1}-1} - (\rho e)_i^n + \frac{\Delta t}{\Delta x}\Delta(u\rho e)\\ &= T_i^n\rho_i^n\frac{R_s}{\gamma_i^{n+1}-1} - \frac{\Delta t}{\Delta x}\left(\frac{\Delta(Tu\rho R_s)}{\gamma^{n+1}-1}\right) - \left(T\rho\frac{R_s}{\gamma-1}\right)_i^n\\ &\quad + \frac{\Delta t}{\Delta x}\Delta\left(Tu\rho\frac{R_s}{\gamma-1}\right)\\ &= \left(\frac{p_i^n}{\gamma_i^{n+1}-1} - \frac{p_i^n}{\gamma_i^n-1}\right) - \frac{\Delta t}{\Delta x}\left(\frac{\Delta(up)}{\gamma_i^{n+1}-1} - \Delta\left(\frac{up}{\gamma-1}\right)\right).\end{aligned} \tag{33}$$

Assuming $\Delta\,(up/(\gamma-1)) \approx \Delta(up)/(\gamma_i^{n+1}-1) + u_i p_i \Delta(1/(\gamma-1))$, the error $(\rho E)_{i_{\text{cons}}}^{n+1}$ is proportional to

$$\frac{1}{\Delta t}\left(\frac{1}{\gamma_i^{n+1}-1} - \frac{1}{\gamma_i^n-1}\right) + \frac{1}{\Delta x}u_i\Delta\left(\frac{1}{\gamma-1}\right). \tag{34}$$

Since Eq. (34) constitutes the explicit discretization of Eq. (27), the conservation error will be small. If T is constant and together with

$$\begin{aligned}(\rho R_s)_i^{n+1} &= R_u\sum_{j=1}^{2}\frac{\rho_{j_i}^{n+1}}{W_j} = R_u\sum_{j=1}^{2}\frac{\rho_{j_i}^n - \dfrac{\Delta t}{\Delta x}\Delta(u\rho_j)}{W_j}\\ &= (\rho R_s)_i^n - \frac{\Delta t}{\Delta x}\Delta(u\rho R_s)\end{aligned}$$

$$\begin{aligned}(\rho c_p)_i^{n+1} &= \sum_{j=1}^{2}\rho_{j_i}^{n+1}c_{p_j} = \sum_{j=1}^{2}\left(\rho_{j_i}^n - \frac{\Delta t}{\Delta x}\Delta(u\rho_j)\right)c_{p_j}\\ &= (\rho c_p)_i^n - \frac{\Delta t}{\Delta x}\Delta(u\rho c_p)\end{aligned}$$

and

$$(\rho c_v)_i^{n+1} = (\rho c_p - \rho R_s)_i^{n+1} = (\rho c_p - \rho R_s)_i^n - \frac{\Delta t}{\Delta x}\Delta(u\rho c_p - u\rho R_s) = (\rho c_v)_i^n - \frac{\Delta t}{\Delta x}\Delta(u\rho c_v)$$

the result (33) reduces to

$$(\rho E)_{i_{error}}^{n+1} = T\left(\frac{\rho_i^{n+1}R_{s_i}^{n+1}}{\gamma_i^{n+1}-1} - \rho_i^{n+1}c_{v_i}^{n+1}\right) = 0.$$

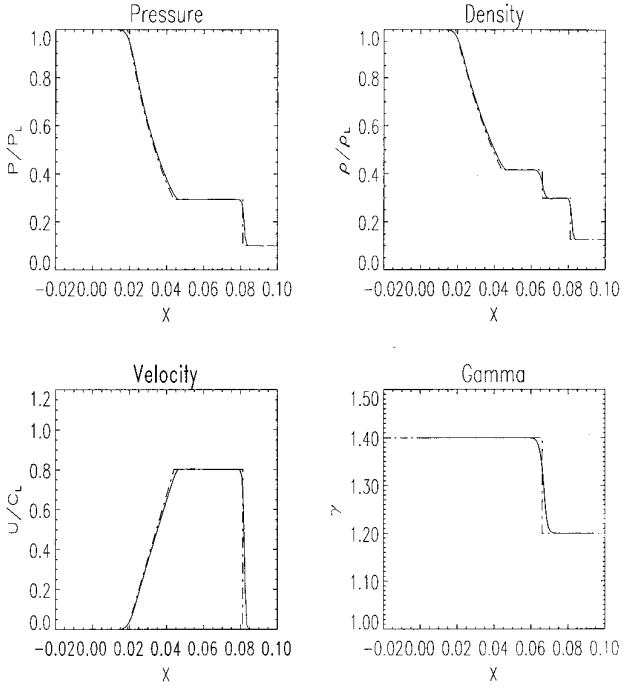

FIG. 5. Riemann problem with correction (100 cells).

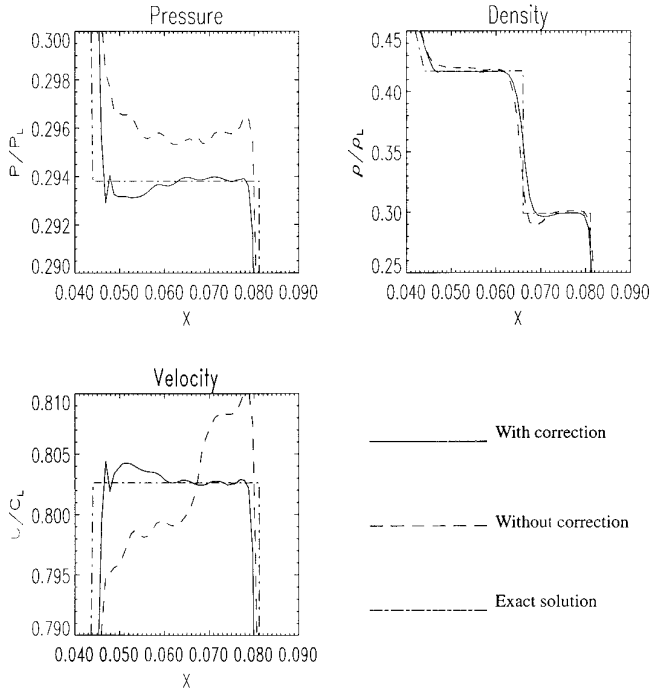

FIG. 6. Comparison of the corrected and the uncorrected solutions with the exact one near the contact discontinuity (100 cells).

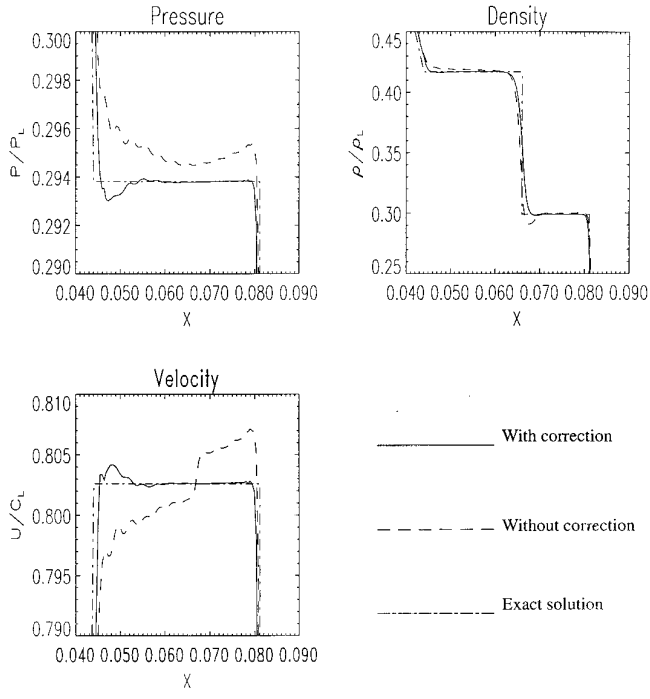

FIG. 7. Comparison of the correct and the uncorrected solutions with the exact one near the contact discontinuity (200 cells).

The same result is obtained with a constant γ. Thus, the conservation error in the energy equation given in Eq. (33) is zero, if the temperature is constant or if γ is constant.

Since ρ_j and ρu are calculated from conservative schemes, there are no conservation errors in the species continuity and momentum equations whatsoever.

6. EXTENSION TO MULTI-DIMENSIONS

To apply the present correction algorithm in 3D, the same procedure can be applied as in 1D. The only thing that changes is the decoding of the conservative variables from the flux, if this is necessary. At the considered cell interface, let $\mathbf{F} = \mathbf{f}(\mathbf{U})s_1 + \mathbf{g}(\mathbf{U})s_2 + \mathbf{h}(\mathbf{U})s_3$ be the known flux. $\mathbf{s} = (s_1, s_2, s_3)^T$ denotes the surface normal of the cell interface in Cartesian coordinates. **f**, **g**, and **h** denote the flux vectors in the x-, y-, and z-directions, respectively, of the 3D Euler equations for two species in Cartesian coordinates. Here we look for the root of the equation $\mathbf{F} = \mathbf{f}(\mathbf{U})s_1 + \mathbf{g}(\mathbf{U})s_2 + \mathbf{h}(\mathbf{U})s_3$ which provides us with the conservative variables for 3D flow at the considered cell interface. This corresponds to six equations for the six unknowns ρ_1, ρ_2, ρu, ρv, ρw, and ρE:

$$F_1 = \mathbf{u} \cdot \mathbf{s}\, \rho_1 \tag{35}$$

$$F_2 = \mathbf{u} \cdot \mathbf{s}\, \rho_2 \tag{36}$$

$$F_3 = \mathbf{u} \cdot \mathbf{s}\, \rho u + p s_1 \tag{37}$$

$$F_4 = \mathbf{u} \cdot \mathbf{s}\, \rho v + p s_2 \tag{38}$$

$$F_5 = \mathbf{u} \cdot \mathbf{s}\, \rho w + p s_3 \tag{39}$$

$$F_6 = \mathbf{u} \cdot \mathbf{s}\, (\rho E + p). \tag{40}$$

If $\mathbf{u} \cdot s = u s_1 + v s_2 + w s_3$, the normal velocity scaled by the area of the cell interface, is not zero, we get as in 1D with Eqs. (4), (35), and (36)

$$(\gamma - 1)^{-1} = \frac{c_p}{R_s} - 1 = \frac{F_1 c_{p_1} + F_2 c_{p_2}}{R_u (F_1/W_1 + F_2/W_2)} - 1. \tag{41}$$

If $\mathbf{u} \cdot \mathbf{s}$ is zero, there is no need in evaluating γ or one of

TABLE I

Total Energy Errors with Corrected and Uncorrected Schemes

No. of cells	Corrected	Uncorrected
50	2.66×10^{-2}	4.69×10^{-2}
100	1.10×10^{-3}	1.43×10^{-2}
200	2.99×10^{-4}	7.57×10^{-3}

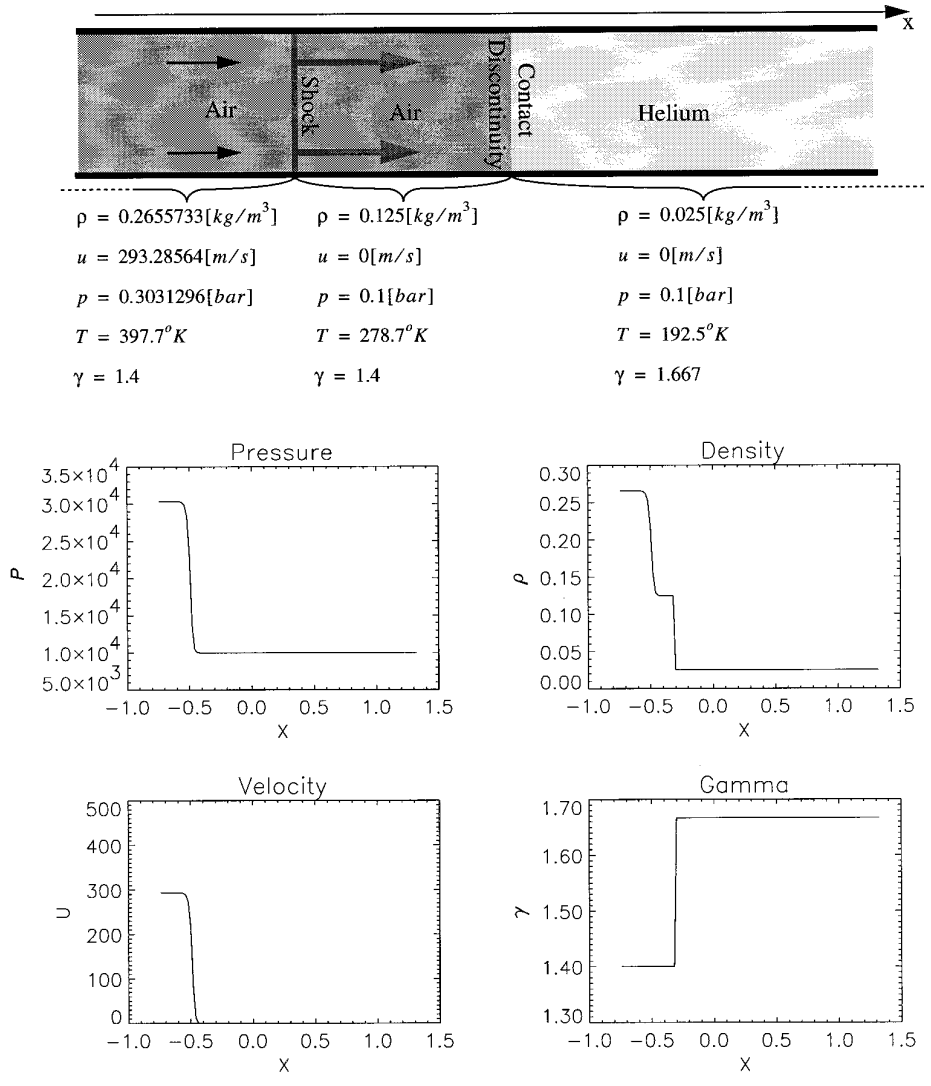

FIG. 8. Initial condition for the interaction of a shock wave with an air/helium contact discontinuity.

the other variables, as the flux in the energy equation is zero. Equations (35) and (36) yield

$$\mathbf{u}\cdot\mathbf{s} = \frac{F_1 + F_2}{\rho}. \tag{42}$$

We define two tangential vectors **a** and **b** of the cell interface such that **s**, **a**, and **b** form an orthogonal basis. For convenience, we scale **a** and **b** such that $|\mathbf{a}| = |\mathbf{b}| = |\mathbf{s}|$.

Forming the scalar products of the momentum flux $\mathbf{G} = (F_3, F_4, F_5)^T$ with **a** and **b**, respectively, we obtain from Eqs. (37), (38), (39), and (42)

$$\mathbf{u}\cdot\mathbf{a} = \frac{\mathbf{G}\cdot\mathbf{a}}{F_1 + F_2} \tag{43}$$

and

$$\mathbf{u}\cdot\mathbf{b} = \frac{\mathbf{G}\cdot\mathbf{b}}{F_1 + F_2}. \tag{44}$$

Once the density is known, the Cartesian velocity components u, v, and w can be determined by solving the linear system (42), (43), (44).

The pressure can be decoded by forming the scalar product of the momentum flux **G** with the surface normal **s** and using Eqs. (37), (38), (39), and (42),

$$p = \frac{\mathbf{G}\cdot\mathbf{s} - (F_1 + F_2)^2/\rho}{\mathbf{s}\cdot\mathbf{s}}. \tag{45}$$

Since $|\mathbf{u}|^2 = ((\mathbf{u}\cdot\mathbf{s})^2 + (\mathbf{u}\cdot\mathbf{a})^2 + (\mathbf{u}\cdot\mathbf{b})^2)/\mathbf{s}\cdot\mathbf{s}$, we get using Eq. (3) applied in 3D,

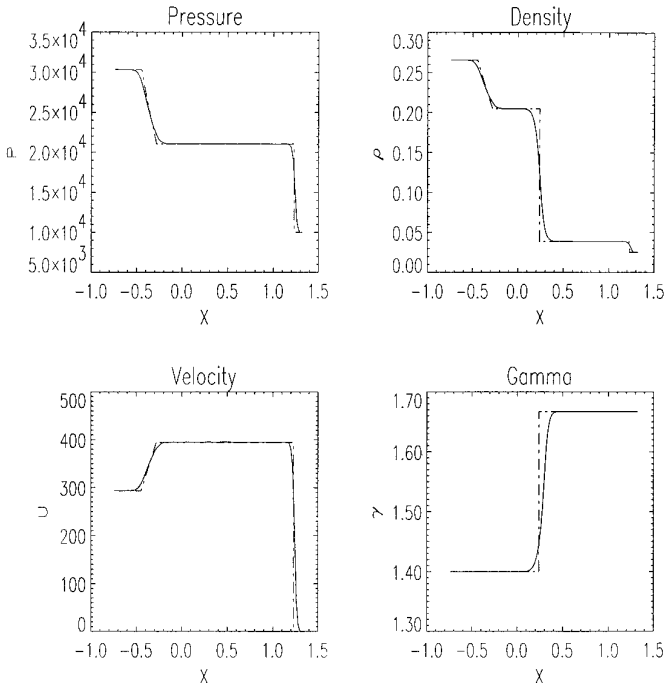

FIG. 9. Interaction of a shock wave with an air/helium contact discontinuity with correction.

$$\rho E = \frac{p}{\gamma - 1} + \frac{\rho}{2}\frac{(\mathbf{u}\cdot\mathbf{s})^2 + (\mathbf{u}\cdot\mathbf{a})^2 + (\mathbf{u}\cdot\mathbf{b})^2}{\mathbf{s}\cdot\mathbf{s}}. \qquad (46)$$

Inserting ρE given by (46) in Eq. (40) and replacing the pressure by (45) and the velocity components by (42), (43), and (44), we obtain a quadratic equation for ρ similar to Eq. (17) with the coefficients

$$\begin{aligned} a &= \frac{F_5}{F_1 + F_2} - \frac{1}{2}\frac{(\mathbf{G}\cdot\mathbf{a})^2 + (\mathbf{G}\cdot\mathbf{b})^2}{(F_1 + F_2)^2\mathbf{s}\cdot\mathbf{s}} \\ b &= \frac{-\gamma}{\gamma - 1}\frac{\mathbf{G}\cdot\mathbf{s}}{\mathbf{s}\cdot\mathbf{s}} \qquad (47) \\ c &= \frac{\gamma + 1}{2(\gamma - 1)}\frac{(F_1 + F_2)^2}{\mathbf{s}\cdot\mathbf{s}}. \end{aligned}$$

Then the density is obtained from Eq. (19).

In 2D the equations simplify, because w, s_3, a_3, F_5, and $\mathbf{G}\cdot\mathbf{b}$ are zero and we can choose $\mathbf{s} = (\Delta y, -\Delta x, 0)^T$ and $\mathbf{a} = (\Delta x, \Delta y, 0)^T$, if $\mathbf{a}$ defines the cell interface. For more than two, say m species, m species mass fluxes instead of the two given by Eqs. (35) and (36) will enter Eqs. (41) to (47).

All the rest remains similar to 1D. Namely the species continuity and momentum equations are discretized as in a conventional finite volume method. Only the discretization of the energy equation is modified by replacing $\gamma^n - 1$ in the cell and at the cell interfaces by $\gamma^{n+1} - 1$ in the cell.

7. RESULTS

Five test cases have been chosen to show the difference between results obtained with and without corrections. The scheme is of second order in space and first order in time. The CFL number is about 0.3.

7.1. *Convection Problem*

The first example is a simple convection problem. A contact discontinuity is transported in a tube. The fluid has initially constant velocity, pressure, and density in the whole tube. The ratio of the temperature of the right and the left sides is 2, and γ is 1.4 on the left and 1.2 on the right side. Figure 3 shows the result after 1, 2, and 3 time steps without correction near the contact discontinuity at $x = 0.045$. The distance 0.09 is discretized by 200 cells. After one time step the velocity is still constant, but there arises a pressure peak as predicted by Eq. (8), which entails a change in velocity. This error increases with time and usually leads to oscillations.

In Figure 4 we can see that we get rid of this error if we apply the correction (Eq. (31)) of the total energy per unit volume. The results after 0, 100, and 200 time steps are plotted and not the slightest oscillations are observed.

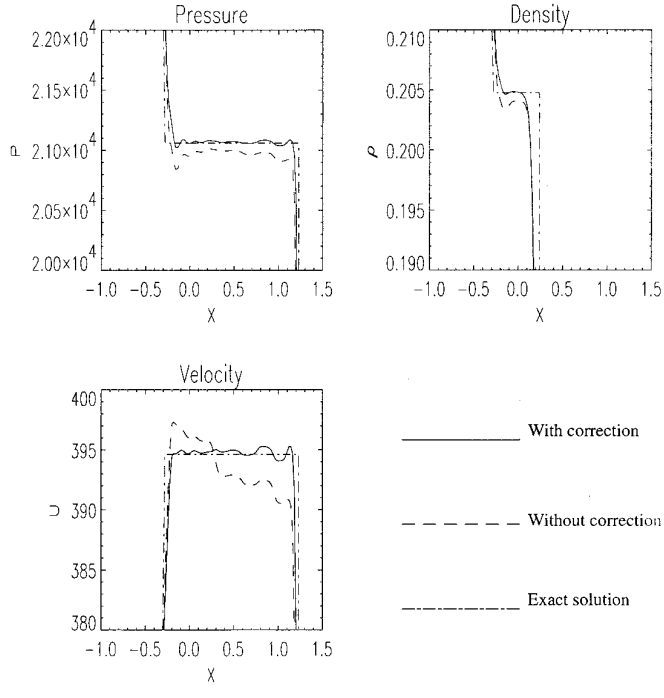

FIG. 10. Comparison of the corrected and the uncorrected solutions with the exact one near the contact discontinuity at $x = 0.23$.

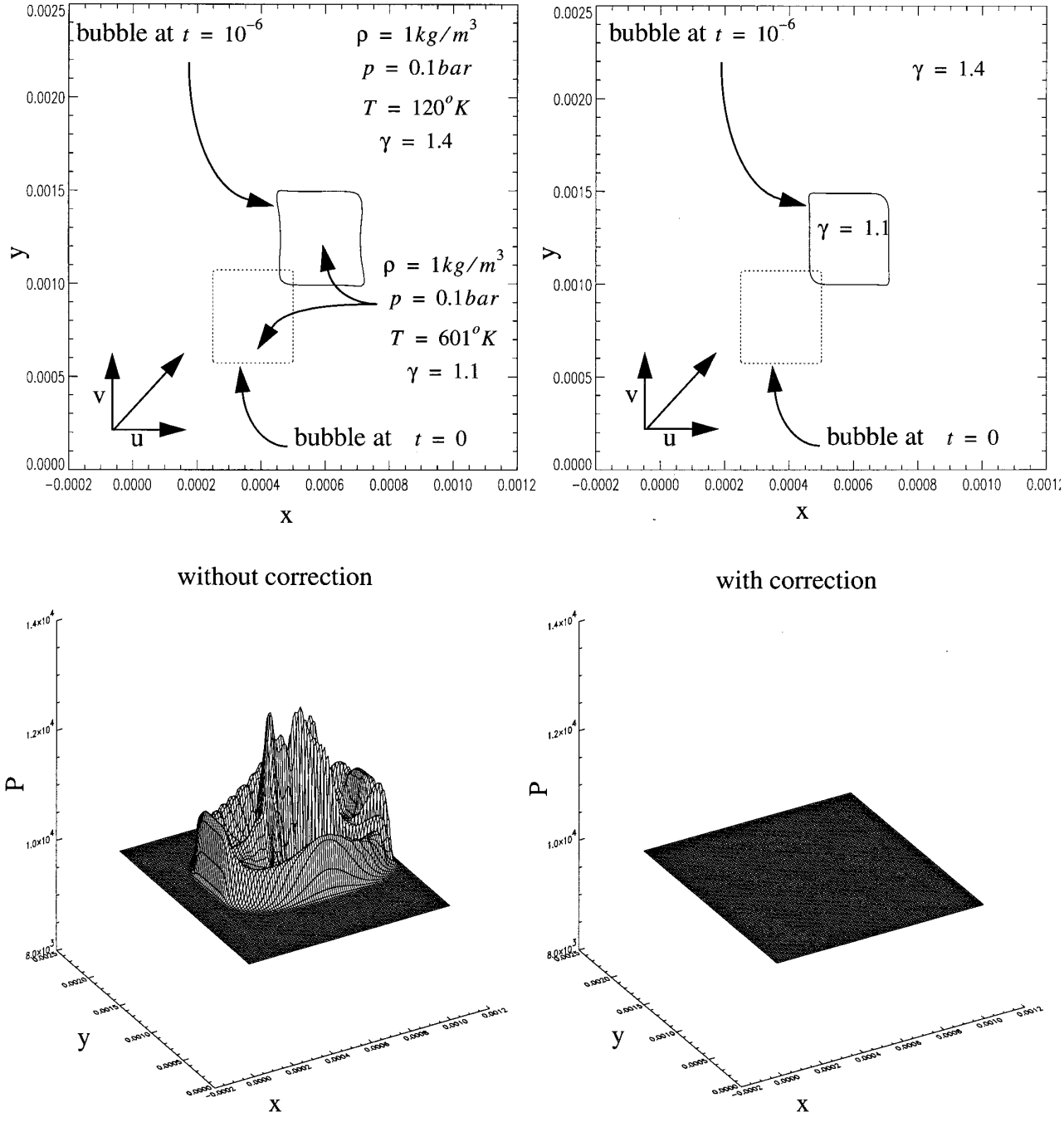

FIG. 11. The 2D convection of a bubble in a supersonic flow (100 × 100 cells).

The plot of γ shows how the contact discontinuity propagates. The velocity and the pressure remain constant. The temperature discontinuity propagates similar to γ.

7.2. *Shock Tube Problem*

The second case is the classical shock tube problem. Initially the velocity is zero in the whole tube, the pressure ratio of the left and right sides is ten, the density on the left side is eight times larger than the density on the right side, the temperature on the right side is 1.6 times higher than on the left side, and γ is 1.4 on the left and 1.2 on the right side [1, 7, 17]. Figure 5 shows the results with the correction (31). The solid lines depict the numerical results after 7×10^{-5}s, while the dashed lines are the exact solutions. The subscript L denotes the initially constant

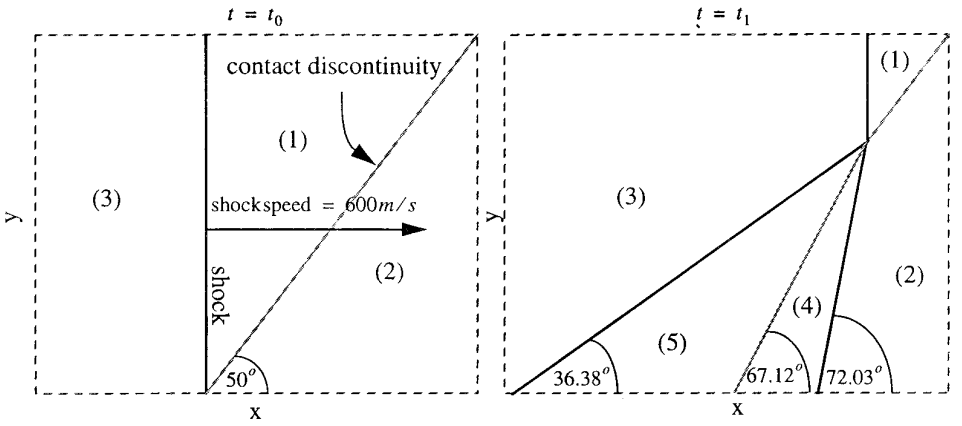

(1):	(2):	(3):	(4):	(5):
$\rho = 1.5556 kg/m^3$	$\rho = 5.1875 kg/m^3$	$\rho = 4.1481 kg/m^3$	$\rho = 24.4293 kg/m^3$	$\rho = 5.0964 kg/m^3$
$u = 0 m/s$	$u = 0 m/s$	$u = 375 m/s$	$u = 262.33 m/s$	$u = 326.19 m/s$
$v = 0 m/s$	$v = 0 m/s$	$v = 0 m/s$	$v = -85.08 m/s$	$v = 66.24 m/s$
$p = 1 bar$	$p = 1 bar$	$p = 4.5 bar$	$p = 6.0092 bar$	$p = 6.0092 bar$
$T = 300.0^o K$	$T = 89.96^o K$	$T = 506.25^o K$	$T = 114.79^o K$	$T = 550.25^o K$
$\gamma = 1.4$	$\gamma = 1.1$	$\gamma = 1.4$	$\gamma = 1.1$	$\gamma = 1.4$

FIG. 12. The 2D test case of the interaction of a planar shock with an oblique contact discontinuity.

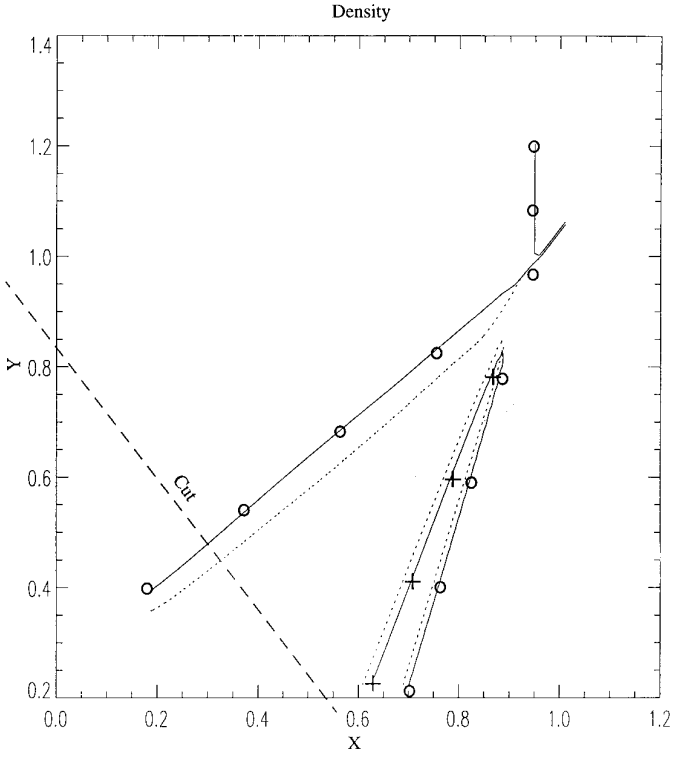

FIG. 13. Comparison of the corrected and the uncorrected density contours of the 2D interaction of a planar shock with an oblique contact discontinuity (100 × 100 cells).

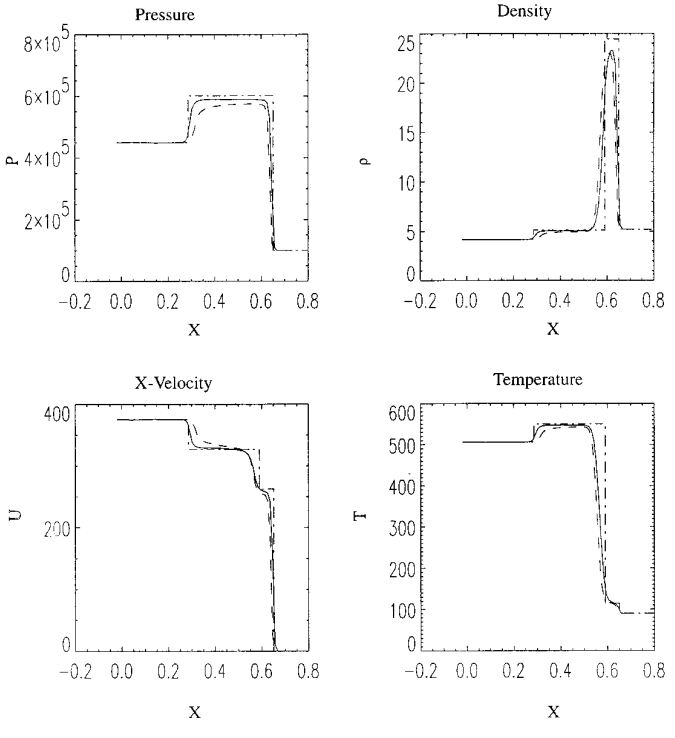

FIG. 14. Comparison of the corrected and the uncorrected 2D solution along a cut diagonal to the grid.

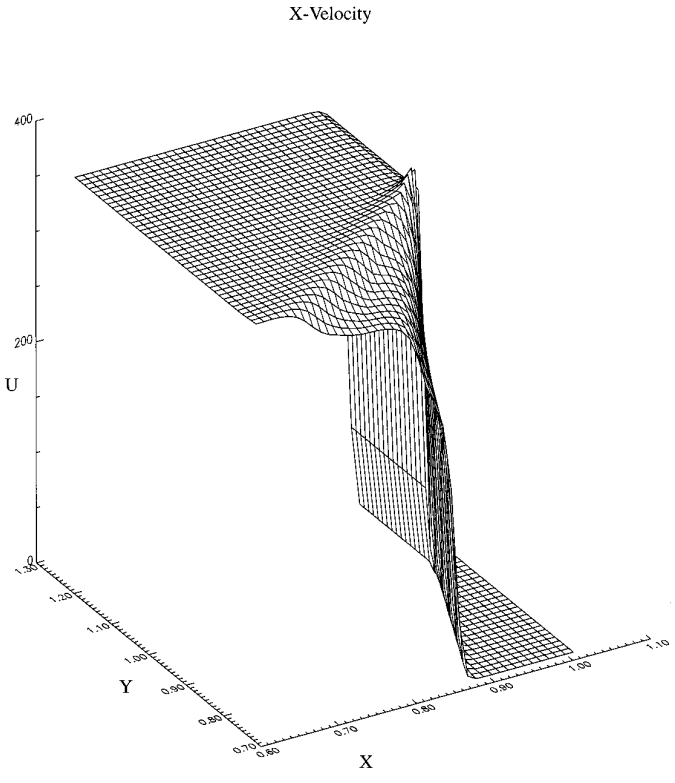

FIG. 15. Surface plot of the x-component of the velocity field near the interaction point without correction.

state of the left hand side of the diaphragm, where we chose $p_L = 1$ bar and $\rho_L = 1$ kg/m^3 and where $c_L = \sqrt{\gamma_L p_L/\rho_L}$ is the speed of sound. The distance 0.09 m is discretized by 100 cells. While the solutions without correction show an error near the contact discontinuity in the velocity and the density plots, which is caused by mixing of species with different γ and temperature, in Fig. 5 almost no error is observed. Figure 6 (100 cells) and Fig. 7 (200 cells) give a closer look near the contact discontinuity. They compare the solutions with and without correction with the exact solution. Without correction, the numerical error near the contact discontinuity is only slightly reduced with mesh refinement. However, with correction that error is almost eliminated on the finer grid. Even near the beginning of the expansion fan, the correction algorithm yields more accurate results than the uncorrected conservative Euler solver.

To show grid convergence, we computed the same shock tube problem on 3 different grids, one with 50 cells, one with 100, and one with 200 cells. In Table I we show the average value of $|(\rho E - \rho E_{\text{exact}})/\rho E_{\text{exact}}|$ between the expansion fan and the contact discontinuity. Table I indicates that the corrected scheme leads to more accurate results than the uncorrected one. Whereas the latter is only first order accurate for the mesh refinement from 100 to 200 cells, the corrected scheme tends to almost second order accuracy.

7.3. *Interaction of a Shock with an Air/Helium Interface*

The third test case considers the interaction of a shock wave with a contact discontinuity. A shock moving with a shock Mach number of 1.65563 from left to right in air hits an air/helium interface (Fig. 8). Related interactions of planar shocks with interfaces were studied in [8]. We initialized the moving shock by using the numerical solutions of the classical shock tube problem, i.e., our second test case in air with $\gamma = 1.4$ on both sides of the diaphragm.

A smeared shock profile with 2 points inside the numerical shock layer was used to avoid the problem of Roe's approximate Riemann solver, which is shared by the Godunov method, with sharp initial conditions for slowly moving shock waves [15]. When using a discontinuous initial shock profile, a velocity overshoot produced in the discrete shock layer in the second time step generated pressure and density valleys and a velocity bump. The pressure and density valleys and the velocity bump travel at the speed $u - c$ of an acoustic wave and another density valley travels at the speed u of a contact discontinuity.

After the interaction of the shock wave with the air/

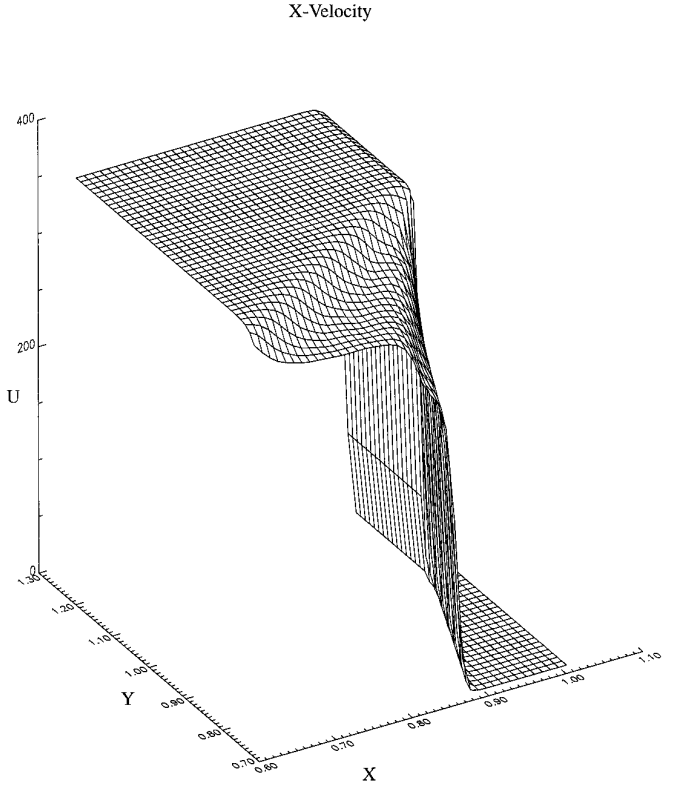

FIG. 16. Surface plot of the x-component of the velocity field near the interaction point with correction.

helium contact discontinuity at $x = -0.3$ m the same wave pattern as for the shock tube problem is observed. Figure 9 shows the computed results with correction after 1.725×10^{-4}s using 100 cells. The dashed lines indicate the exact solution. A closer look at velocity and pressure near the contact discontinuity (Fig. 10) shows the improved results due to the correction algorithm. The error of the conservative scheme in velocity and pressure near the air/helium interface is almost eliminated with the correction. Note that the slope of the velocity of the uncorrected conservative scheme near the contact discontinuity for the third test case with $\gamma_L < \gamma_R$ (Fig. 10) is of opposite sign compared with the corresponding result for the second test case where $\gamma_L > \gamma_R$ (Figs. 6 and 7). Without correction, the pressure near the contact discontinuity is predicted too small for $\gamma_L < \gamma_R$ (Fig. 10), whereas for $\gamma_L > \gamma_R$ the uncorrected pressure is too large (Figs. 6 and 7) confirming the analysis of Section 4 because $T_R > T_L$ in both cases. Since the error in density of the uncorrected conservative scheme is largest at the beginning of the expansion fan, we present the comparison of the density near that region illustrating the improvement by the correction algorithm (Fig. 10). The contact discontinuity in the density plot of this figure seems to be in the wrong location because we zoomed in on the higher values of density. In fact the contact discontinuity is symmetrically smeared about the correct location (Fig. 9). The waves between the shock and the expansion fan (Fig. 10) seem to be of the same origin as the ones described for the incident shock above. In summary, the improved results near the air/helium interface demonstrate that the correction algorithm also works for the interaction of a shock wave with a contact discontinuity.

7.4. *Convection of a Fluid Bubble in 2D*

As in our first 1D test case, we look at a field of constant pressure and velocity (Fig. 11). But within a quadratic bubble of different fluid, the ratio of specific heats γ and the temperature are different from those of the surrounding fluid. This time we have supersonic flow at $M = 1.89$, but again we expect that pressure and velocity remain constant and that the bubble moves with the velocity of the fluid. If we apply a conservative scheme without any correction, we run into the same problem we outlined before (Fig. 11, left side) and which we can eliminate by applying our correction (Fig. 11, right side). The dashed lines in Fig. 11 show the initial location of the bubble, whereas the solid lines show the contour line $\gamma = 1.25$ after 10^{-6}s.

7.5. *2D Interaction of a Shock with a Contact Discontinuity*

The fifth test case is a 2D interaction of a planar shock with an oblique contact discontinuity. We have chosen this test case because there exists an exact solution to compare with. The shock Mach number is 2. The initial conditions and the exact solution are sketched in Fig. 12. The results shown in Figs. 13–18 were obtained on a 100×100 grid ($\Delta y = \Delta x \tan(50°)$) after 500 time steps corresponding to $t = 0.00125$ s after the beginning of the simulated interaction. The solid density contours of the levels 3 kg/m^3, 4.5 kg/m^3, and 15 kg/m^3 in Fig. 13 represent the result obtained with the corrected scheme, and the dashed contours those of the uncorrected one. The markers indicate the exact

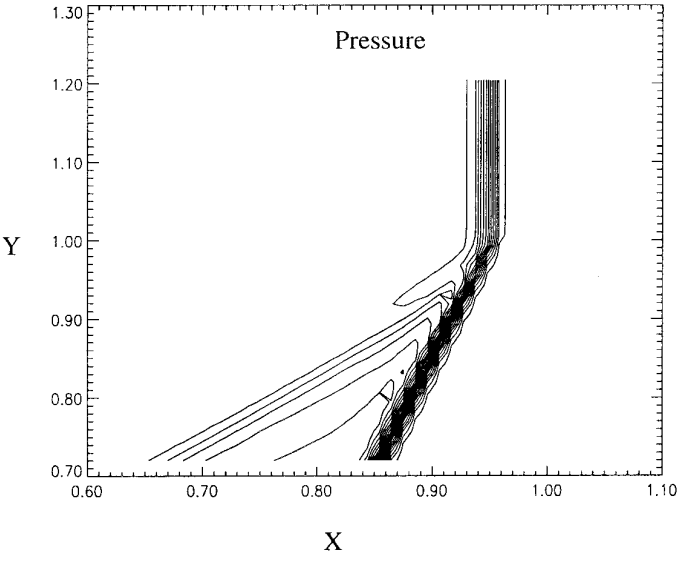

FIG. 17. Contour plot of the pressure near the interaction point without correction.

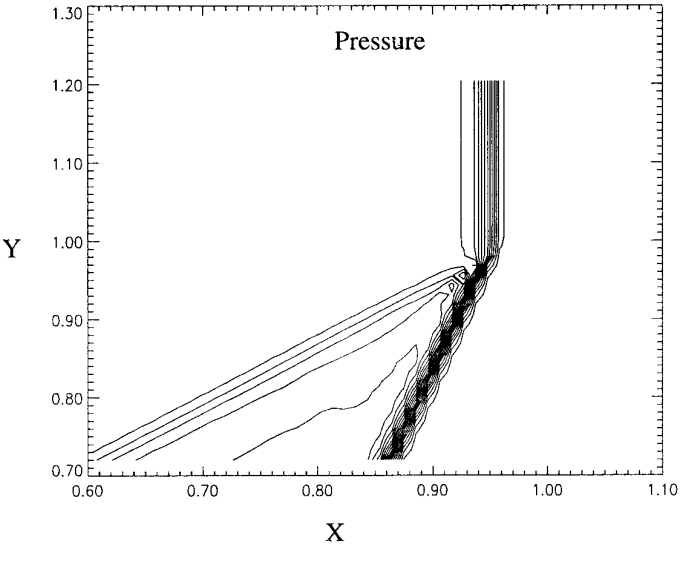

FIG. 18. Contour plot of the pressure near the interaction point with correction.

solution. The + shows the contact discontinuity, whereas the o stands for the shocks. Figure 14 shows the profiles of the pressure, the density, the x-component of the velocity, and the temperature along a cut diagonal to the grid lines (Fig. 13), where the solid lines represent the corrected solution and the dashed lines the uncorrected one. The dashed pointed lines show the exact solution. Again the corrected results are more accurate than the uncorrected ones. Finally Figs. 15, 16, 17, and 18 give a closer look at the neighborhood of the interaction point, where the 5 regions meet. Figures 15 and 16 show surface plots of the x-component of the velocity. The results of the uncorrected computation (Fig. 15) show an overshoot near the interaction point, but not so those of the computation with the correction (Fig. 16). Figures 17 and 18 show 20 contour lines of the pressure. Whereas the reflected shock is in a wrong location without correction (Figs. 17 and 13), it is in the correct location with correction (Figs. 18 and 13).

8. CONCLUSIONS

Inviscid flow of perfect gas mixtures has been calculated with a conservative scheme. To avoid oscillations occurring at contact discontinuities, where the temperature and γ, the ratio of specific heats, are not constant, a correction algorithm of the total energy per unit volume has been developed, analyzed, and tested. It can easily be built into any explicit code which uses a conservative formulation. The 1D and 2D test cases for mixtures of two perfect gases show that the correction algorithm really corrects inaccuracies at convected contact discontinuities and allows much more accurate computations of shock tube problems and shock interface interactions. The straightforward extension of the algorithm to 3D and several species has been outlined.

Since the correction procedure needs the flow variables at the volume interfaces, we have shown how to decode the fluxes.

ACKNOWLEDGMENT

The authors thank the referees for their valuable comments, which helped to improve the article.

REFERENCES

1. R. Abgrall, Generalization of Roe's Riemann solver to mixtures of perfect gas, *Rech. Aérospat.* **6,** 31 (1988).
2. R. Abgrall, How to prevent pressure oscillations in multicomponent flow calculations: A quasi conservative approach, *J. Comput. Phys.* **125,** 150 (1996).
3. P. Colella, H. M. Glaz, and R. E. Ferguson, Multifluid algorithms for Eulerian finite difference methods, unpublished manuscript, 1989.
4. B. Einfeldt, C. D. Munz, P. L. Roe, and B. Sjögreen, On Godunov-type methods near low densities, *J. Comput. Phys.* **92,** 273 (1991).
5. G. Fernandez and B. Larrouturou, Hyperbolic schemes for multicomponent Euler equations, in *Nonlinear Hyperbolic Equations—Theory, Computational Methods and Applications,* edited by J. Ballmann and R. Jeltsch, Notes Numer. Fluid Mech., Vol. 24 (Vieweg, Braunschweig, 1989), p. 128.
6. A. Harten, High resolution schemes for hyperbolic conservation laws, *J. Comput. Phys.* **49,** 357 (1983).
7. S. Karni, Multicomponent flow calculations by a consistent primitive algorithm, *J. Comput. Phys.* **112,** 31 (1994).
8. S. Karni, Hybrid multifluid algorithms, *SIAM J. Sci. Statist. Comput.* **17** (5), 1019 (1996).
9. Y. Liu and M. Vinokur, Upwind algorithms for general thermochemical nonequilibrium flows, AIAA Paper 89-0201, 1989.
10. E. S. Oran and J. P. Boris, *Numerical Simulation of Reactive Flow* (Elsevier, New York, 1987).
11. M. Pandolfi, A contribution to the numerical prediction of unsteady flows, *AIAA J.* **22** (5), 602 (1984).
12. C. Park, *Nonequilibrium Hypersonic Aerothermodynamics* (Wiley, New York, 1990).
13. J. J. Quirk and S. Karni, On the dynamics of a shock-bubble interaction, *J. Fluid Mech.* **318,** 129 (1996).
14. P. L. Roe, Approximate Riemann solvers, parameter vectors, and difference schemes, *J. Comput. Phys.* **43,** 357 (1981).
15. T. W. Roberts, The behavior of flux difference splitting schemes near slowly moving shock waves, *J. Comput. Phys.* **90,** 141 (1990).
16. A. H. Shapiro, *The Dynamics and Hydrodynamics of Compressible Fluid Flow* (Ronald Press, New York, 1953), Vol. 1.
17. E. F. Toro, Defects of conservative methods and adaptive primitive conservative schemes for computing solutions to hyperbolic conservation laws, Tech. Rep. MMU-9401, Department of Mathematics and Physics, Manchester Metropolitan University, December 1994 (unpublished).
18. R. W. Walters, P. Cinella, D. C. Slack, and D. Halt, Characteristic-based algorithms for flows in thermochemical nonequilibrium, *AIAA J.* **30** (5), 1304 (1992).